Magnetic Resonance Imaging 32 (2014) 1344–1352

Contents lists available at ScienceDirect

Magnetic Resonance Imaging

journal homepage: www.mrijournal.com

Fast multi-contrast MRI reconstruction

Junzhou Huang [a,*], Chen Chen [a], Leon Axel [b]

[a] Department of Computer Science, Engineering, University of Texas at Arlington, 500 UTA Boulevard, Arlington, TX 76019, United States
[b] Department of Radiology, New York University, New York, NY 10016, United States

ARTICLE INFO

Article history:
Received 6 March 2014
Revised 27 July 2014
Accepted 9 August 2014

Keywords:
Compressed sensing MRI
Multi-contrast MRI
Joint sparsity
Joint total variation

ABSTRACT

Multi-contrast magnetic resonance imaging (MRI) is a useful technique to aid clinical diagnosis. This paper proposes an efficient algorithm to jointly reconstruct multiple T1/T2-weighted images of the same anatomical cross section from partially sampled *k*-space data. The joint reconstruction problem is formulated as minimizing a linear combination of three terms, corresponding to a least squares data fitting, joint total variation (TV) and group wavelet-sparsity regularization. It is rooted in two observations: 1) the variance of image gradients should be similar for the same spatial position across multiple contrasts; 2) the wavelet coefficients of all images from the same anatomical cross section should have similar sparse modes. To efficiently solve this problem, we decompose it into joint TV regularization and group sparsity subproblems, respectively. Finally, the reconstructed image is obtained from the weighted average of solutions from the two subproblems, in an iterative framework. Experiments demonstrate the efficiency and effectiveness of the proposed method compared to existing multi-contrast MRI methods.

1. Introduction

Magnetic resonance imaging (MRI) has been widely used to visualize the same anatomical cross section under multiple contrast settings, since the multi-contrast MR images can achieve superior power for clinical diagnosis over individual T1, T2 or proton-density weighted images. Recently, compressive sensing (CS) theory [1,2] has been successfully applied to accelerate MRI scanning [3–6]. These conventional CS-MRI methods can reconstruct an MR image from undersampled *k*-space data by utilizing the sparsity of the image in both wavelet and gradient domains. However, all these methods have previously been used to reconstruct T1, T2 or proton-density weighted images individually while ignoring the spatial similarity across different contrasts. No structured prior information has been exploited in these methods other than sparsity for multi-contrast MRI.

Guided by CS theory [1,2], the necessary measurement number is $\mathcal{O}(TK + TK\log(N/K))$ if we directly apply CS-MRI methods [3–6] to reconstruct each multi-contrast MR image individually. Here, T is the contrast number, K is the sparsity number and N is the pixel number. However, the multi-contrast MR images are not independent, but rather are highly correlated, as they are acquired from the same anatomical cross section. They have the same tissue boundaries, although the pixels values may differ in different image contrasts. This implies the magnitude of the gradients at same spatial location should be zeros or non-zeros simultaneously across multiple contrasts. Their wavelet coefficients follow a similar pattern. Therefore, they should be group sparse on the wavelet or gradient domain, not only standard sparse. According to the group sparsity theory for CS [7–9], the necessary measurement number can be reduced to $\mathcal{O}(TK + K\log(N/K))$ instead of $\mathcal{O}(TK + TK\log(N/K))$. Intuitively, the multi-contrast images are preferred to be reconstructed jointly.

There are many algorithms that have been proposed for the group sparsity problem in the literature (e.g. Refs. [10–13]). However, they have rarely been validated on multi-contrast MRI, where the sampling matrices are partial Fourier transforms with different frequency sets. In multi-contrast MRI, although group sparsity has been exploited in wavelet domain to achieve better results than standard sparsity [14–16], the group sparsity of the gradients has not been generally considered. Although group sparsity on gradients of multi-contrast MRI is exploited under a multi-task Bayesian framework [17], it is unknown how to couple group wavelet-sparsity into their method. Unfortunately, no work has fully utilized the benefits of group sparsity on both domains so far. In addition, all the previous algorithms [10–14,17] are generally very slow due to high computational complexity in each iteration. The limitations on both accuracy and reconstruction time make it difficult to use multi-contrast CS-MRI in clinic applications.

Motivated by the above short comings in multi-contrast MRI, we here propose a fast method to jointly reconstruct T1, T2 and proton-density weighted images by fully exploiting the group sparsity on both wavelet and gradient domains over multi-contrast data

* Corresponding author.
E-mail address: jzhuang@uta.edu (J. Huang).

http://dx.doi.org/10.1016/j.mri.2014.08.025
0730-725X/

acquisitions. The reconstruction problem is formulated as minimizing a linear combination of three terms, corresponding to a least squares data fitting, joint total variation (JTV) and group wavelet-sparsity regularization. A novel algorithm is developed to efficiently solve this problem. There are three key features of our algorithm for multi-contrast MRI: first, the group sparsity in both wavelet and gradient domains are exploited, which is not feasible for existing algorithms [14,17]. Second, our algorithm is accelerated by FISTA [18,19] which meets the optimal convergence rate for first order methods. Finally, the computational complexity of each iteration in our algorithm is $\mathcal{O}(TNlogN)$, which demonstrates the efficiency of the proposed method. Extensive experiments validate the superiority of the proposed method in both reconstruction accuracy and computational complexity. Preliminary results of this paper have appeared in a conference paper presented at MICCAI 2012 [20].

2. Theory

2.1. Compressive sensing MRI

Compressive sensing has received abundant attention in the MRI community since it is first studied in MRI by Lustig et al. [3]. The MR image reconstruction process can be formulated as:

$$\hat{x} = arg\min_x \left\{ \frac{1}{2}\|Fx-b\|^2 + \alpha\|x\|_{TV} + \beta\|\Phi x\|_1 \right\} \quad (1)$$

where x is an MR image to be reconstructed, F is the undersampled Fourier transform, y is the vector of k-space measurements, Φ is the wavelet basis, $\|x\|_{TV}$ is the total variation defined as $\|x\|_{TV} = \sum_{i=1}^{N}\sqrt{\left((\nabla_1 x_i)^2 + (\nabla_2 x_i)^2\right)}$. Here, ∇_1 and ∇_2 denote the forward finite difference operators on the first and second coordinates and are two parameters to be tuned. This classical CS-MRI model was first solved by a nonlinear conjugate gradient method (CG) in SparseMRI [3]. A positive smoothing parameter is used to convert the non-smooth terms to smooth ones, and then the gradient of the function can be derived. TVCMRI [4] and RecPF [5] used an operator-splitting method and a variable splitting method to solve this problem, respectively. They have much lower computational cost than CG in each iteration. FCSA [6] decomposed this problem into two simpler problems and then accelerated them with FISTA [18,19] respectively. The results can be further improved by exploiting the complex structure of wavelet coefficients [21,22]. These are current state-of-the-art algorithms for solving the CS-MRI problem (1). However, they can only reconstruct T1, T2 or proton-density weighted images individually, without exploiting their spatial joint structure. In this study, we assume the wavelet basis is orthogonal. For non-orthogonal wavelet basis, some synthesis and analysis prior based algorithms can be used to solve the problem [23–25].

2.2. The benefit of group sparsity

CS theory suggests that if the signal is sparse, it can be exactly recovered with a sub-Shannon/Nyquist sampling ratio. However, this requires the sampling matrix satisfies the restricted isometry property (RIP) [1,2]. To ensure that the sampling matrix satisfies the RIP with high probability, the number of measurements should be at least $\mathcal{O}(K + Klog(N/K))$. This is a minimum bound for sparse signals. Nevertheless, the number of measurements could be reduced by utilizing the underlying structures in the signal. For example, some signals have group sparse priors, which means that the coefficients of the signal tend to cluster in groups, and each group contains zero-coefficients or non-zero coefficients only. Recently, structured sparsity theories proved that only $\mathcal{O}(K + qlog(N/q))$ measurements are required for the group sparse signal [7–9], where $q = K/g$ and g denotes the number of groups. To utilize the group sparsity, $\ell_{2,1}$ norms are often used instead of ℓ_1 norms. By geometric interpretation, the ℓ_1 norm ball has some singular values at the axes, which encourages sparseness. The singular values appear on the $\ell_{2,1}$ norm ball only when all coordinates in the same group are zeros simultaneously [13,26]. Intuitively, this encourages group sparsity. For the multi-contrast MRI problem with T contrast settings, at least $\mathcal{O}(TK + TKlog(N/K))$ samples are required by conventional CS-MRI methods. As the images structures tend to have an underlying similarity across multi-contrast images, the coefficients at the same locations across multi-contrast images tend to be group sparse. Therefore, only $\mathcal{O}(TK + Klog(N/K))$ samples are required, based on the structured sparsity theories. Alternatively, with the same density of sampling, more accurate reconstructions can be achieved.

2.3. Proposed fast multi-contrast reconstruction

In the multi-contrast imaging setting, the different MR images denote MRI scans with different imaging weights. We make two observations about them: 1) the relative magnitudes of the gradients of images should be similar for the same spatial positions across multiple contrasts; and 2) the wavelet coefficients of all MR images from the same spatial positions should have similar sparse modes. Intuitively, better performance can be achieved by fully exploiting group sparsity in both the wavelet and gradient domains. Motivated by these considerations, the joint reconstruction problem can be formulated as follows:

Algorithm 1. Proposed FCSA-MT

Input: $\rho = \frac{1}{L_f}$, α, β, $t^1 = 1$ $Z = X^0$
for $k = 1$ **to** K **do**
  $Y = Z - \rho\nabla f(Z)$, $s = 1, \ldots, T$
  $X_1 = argmin_X\left\{\frac{1}{4\rho}\|X-Y\|^2 + \alpha\|X\|_{JTV}\right\}$
  $X_2 = argmin_X\left\{\frac{1}{4\rho}\|X-Y\|^2 + \beta\|\Phi X\|_{2,1}\right\}$
  $X^k = \frac{X_1+X_2}{2}$; $t^{k+1} = \frac{1+\sqrt{1+4(t^k)^2}}{2}$
  $Z = X^k + \frac{t^k-1}{t^{k+1}}\left[X^k - X^{k-1}\right]$
end for

$$\hat{X} = arg\min_X \left\{ F(x) = \frac{1}{2}\sum_{s=1}^{T}\|F_s X(:,s) - y_s\|^2 + \alpha\|X\|_{JTV} + \beta\|\Phi X\|_{2,1} \right\} \quad (2)$$

where $X = [x_1, x_2, x_T]$ is the set of all multi-contrast images, and F_s and y_s are the sampling matrix and k-space measurements for the s-th image, respectively. The $\ell_{2,1}$ norm is defined as $\|X\|_{2,1} = \sum_{i=1}^{N}\left(\sqrt{\sum_{s=1}^{T}(\Phi X_{is})^2}\right)$, which is the summation of the ℓ_2 norm for each row. $\|X\|_{JTV} = \sum_{i=1}^{N}\sqrt{\sum_{s=1}^{T}\left((\nabla_1 X_{is})^2 + (\nabla_2 X_{is})^2\right)}$. The JTV is also known as color total variation for color image denoising [27,28]. To solve problem (2), we follow the FCSA [6] scheme to decompose it into two subproblems. Let $f(X) = \frac{1}{2}\sum_{s=1}^{T}\|F_s X_s - y_s\|_2^2$, $g_1(X) = \alpha\|X\|_{JTV}$ and $g_2(X) = \beta\|\Phi X\|_{2,1}$. Algorithm 1 outlines the whole algorithm for this problem. Here, $\nabla f(X)$ denotes the gradient of $f(X)$ and L_f denotes its Lipschitz constant.

For the subproblem of X_2:

$$X_2 = arg\min_X \left\{ \frac{1}{4\rho}\|X-Y\|^2 + \beta\|\Phi X\|_{2,1} \right\} \quad (3)$$

there is a closed form solution, by soft thresholding:

$$(X_2)_i = \Phi^T\left(max\left(1-\frac{2\rho\beta}{||(\Phi X)_i||_2},0\right)(\Phi X)_i\right) \tag{4}$$

where $(\cdot)_i$ denotes the i-th row of the matrix. The efficiency of the whole algorithm is highly dependent on how quickly we can solve the X_1 subproblem in each iteration.

For the subproblem of X_1:

$$X_1 = arg\min_X\left\{\frac{1}{4\rho}||X-Y||^2+\alpha||X||_{JTV}\right\} \tag{5}$$

There is no closed form solution. The Fast Gradient Projection (FGP) algorithm for TV [19] previously proposed cannot directly solve it, due to the different formulation. Fortunately, we have developed a new method, called Fast Joint-Gradient Projection (FJGP) algorithm, for this JTV problem. Following FGP [19], we consider a dual method for problem (5). Supposing the size of each image is m by n with $m \times n = N$, we reshape the image matrices X, Y to $m \times n \times T$ for convenience. Let P be a $(m-1) \times n \times T$ matrix, Q be a $m \times (n-1) \times T$ matrix, and that they satisfy:

$$\begin{cases} \sum_{s=1}^{T}\left(P_{i,j,s}^2+Q_{i,j,s}^2\right)\le 1 & i=1,2,\ldots,m-1; j=1,2,\ldots,n-1 \\ |P_{i,n,s}|\le 1 & i=1,2,\ldots,m-1; s=1,2,\ldots,T \\ |Q_{m,j,s}|\le 1 & j=1,2,\ldots,n-1; s=1,2,\ldots,T \end{cases} \tag{6}$$

A linear operator is defined as $\mathscr{L}(P, Q)_{i,j,s} = P_{i,j,s} - P_{i-1,j,s} + Q_{i,j,s} - Q_{i,j-1,s}$ where $i = 1, \ldots, n_1, j = 1, \ldots, n_2$, and $s = 1, \ldots, T$. The $\mathscr{L}^T$ is defined as $\mathscr{L}^T(X) = (P, Q)$, where $P \in \mathbf{R}^{(n_1-1)\times n_2\times T}$ and $Q \in \mathbf{R}^{n_1\times(n_2-1)\times T}$. Therefore, the optimal solution for problem (5) is $X^* = Y - 2\alpha\rho\mathscr{L}(P^*, Q^*)$, where (P^*, Q^*) is the optimal solution for

$$\min_{P,Q}\left\{h(P,Q) = Y-2\alpha\rho\mathscr{L}(P,Q)_F^2\right\} \tag{7}$$

where $||\cdot||_F$ denotes the Frobenius norm. Note that problem (7) could be accelerated by FISTA [19]. The whole algorithm for problem (5) is summarized in Algorithm 2. Our recent study shows that the JTV can also improve parallel MRI reconstruction [29].

Algorithm 2. Proposed FJGP for joint total variation

Input: ρ, α, Y, P^0, Q^0, U, V
for $k = 1$ **to** K **do**
  $t^{k+1} = \frac{1+\sqrt{1+4(t^k)^2}}{2}$
  for $s = 1$ **to** T **do**
    $\left(P^k, Q^k\right) = \text{Proj}\left[(U,V)+\frac{1}{16\rho\alpha}\mathscr{L}^T[Y-2\rho\alpha\mathscr{L}(U,V)]\right]$
    $(U,V) = \left(P^k, Q^k\right)+\frac{t^k-1}{t^{k+1}}\left(P^k-P^{k-1}, Q^k-Q^{k-1}\right)$
  end for
end for
$X = Y - 2\rho\alpha\mathscr{L}(P^K, Q^K)$

The projection operator $\text{Proj}(P, Q) = (U, V)$ is used to force (P,Q) to satisfy the condition (6):

$$U_{i,j,s} = \begin{cases} \dfrac{P_{i,j,s}}{max\left(1,\sqrt{\sum_{s=1}^{T}P_{i,j,s}^2+Q_{i,j,s}^2}\right)} & i=1,2,\ldots,m-1; j=1,2,\ldots,n-1 \\ \dfrac{P_{i,n,s}}{max\left(1,\sqrt{\sum_{s=1}^{T}P_{i,n,s}^2}\right)} & i=1,2,\ldots,m-1 \end{cases} \tag{8}$$

and

$$V_{i,j,s} = \begin{cases} \dfrac{Q_{i,j,s}}{max\left(1,\sqrt{\sum_{s=1}^{T}P_{i,j,s}^2+Q_{i,j,s}^2}\right)} & i=1,2,\ldots,m-1; j=1,2,\ldots,n-1 \\ \dfrac{Q_{m,j,s}}{max\left(1,\sqrt{\sum_{s=1}^{T}Q_{m,j,s}^2}\right)} & j=1,2,\ldots,n-1 \end{cases} \tag{9}$$

It can be observed that all operations in Algorithm 2 are linear. Therefore the total computational complexity is $\mathcal{O}(TN)$. It can be easily proved that Algorithm 2 achieves the optimal convergence rate $F\left(X^k\right)-F(X^*)\le\mathcal{O}\left(1/k^2\right)$ [17,18]. Due to the tradeoff between efficiency and effectiveness, the FJGP algorithm only runs for 1 iteration in our implementation. For the entire Algorithm 1, step 1 takes $\mathcal{O}(TNlogN)$ if the fast Fourier transform (FFT) is applied. Steps 2 and 3 for the two subproblems take $\mathcal{O}(TN)$. Therefore, the computational complexity for the whole algorithm is $\mathcal{O}(TNlogN)$. In addition, it is accelerated by FISTA, which has very fast convergence speed.

3. Method

The proposed method was evaluated on three datasets: the SRI24 brain atlas [30], the complex-valued Shepp–Logan phantom data, and in vivo brain data. All reconstruction methods were implemented in MATLAB (MathWorks, Natick, MA) on a desktop computer with an Intel i7-3770 central processing unit and 12-GB random-access memory. We compared our algorithm with conventional CS-MRI methods SparseMRI [3], TVCMRI [4], RecPF [5], FCSA [6], and multi-contrast MRI methods Bayesian CS (BCS) [17] and GroupSparseMRI [14] (we call it GSMRI for short). For fair comparison, all codes were downloaded from the authors' websites and we carefully followed their experiment setup. All the convex relaxation methods were run for 100 iterations and the parameters were set the same for them. Due to the slow convergence speed of Bayesian CS (e.g., 26.4 hours for the SRI24 brain atlas [30]), we only ran it for 6000 iterations as we are interested in fast reconstruction. The BCS method has been accelerated in a recent work [31], but it still requires 9 min to reconstruct the images. The accelerated version is much less accurate than the original version and is therefore not compared. We added Gaussian white noise with 0.01 standard deviation for the simulated data. The images with Nyquist rate sampling were used as reference images. Signal-to-noise ratio (SNR) and relative error (RE) were used for result evaluation. $\text{SNR} = 10log10(V_s/V_n)$, where V_n is the mean square error between the reference image x_0 and the reconstructed image x; $V_s = \text{var}(x_0)$ denotes the power level of the original image, where $\text{var}(x_0)$ denotes the variance of the values in x_0. $\text{RE} = 100\,\% \times ||x - x_0||_2/||x_0||_2$.

3.1. SRI24 multi-channel brain atlas data

This experiment was conducted on an MR image extracted from the SRI24 atlas [30].The atlas features structural scans were obtained on a 3.0 T GE scanner with an 8-channel head coil with three different contrast settings:

i For T1-weighted structural images: 3D axial IR-prep SPoiled Gradient Recalled (SPGR), TR = 6.5 ms, TE = 1.54 ms, number of slices = 124, slice thickness = 1.25 mm.
ii For proton density-weighted (early-echo) and T2-weighted (late-echo) images: 2D axial dual-echo fast spin echo (FSE), TR = 10,000 ms, TE = 14/98 ms, number of slices = 62, slice thickness = 2.5 mm.

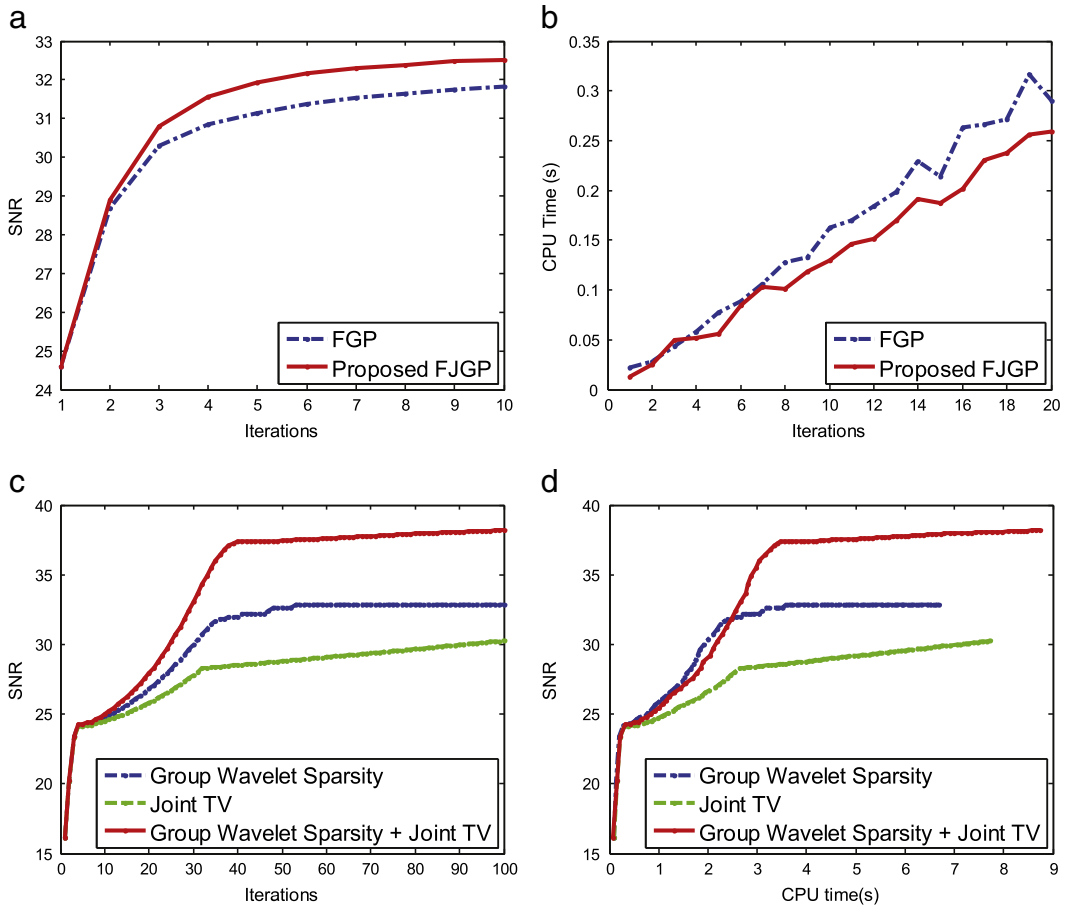

Fig. 1. Demonstration of the benefit of the proposed method for SRI24 dataset. a: The SNRs of the denoising result with FPG [19] and the proposed FJPG. b: Comparison of the computational time between FPG [19] and the proposed FJPG. c: Comparison of the SNR in terms of iterations among only group wavelet sparsity, only joint TV, and their combination. d: Comparison of the SNR in terms of CPU time among only group wavelet sparsity, only joint TV, and their combination.

The field-of-view covers a region of 240 × 240 mm with resolution 256 × 256 pixels. The sampling mask is Gaussian random with variable density and reduction factor $R = 4$. More samples were acquired at low frequencies and fewer samples were acquired at higher frequencies [3,6]. Reconstructions were performed using conventional CS-MRI methods [3–6], multi-contrast MRI methods [17,14] and the proposed. All the convex relaxation methods ran for 100 iterations and BCS ran for 6000 iterations, due to its higher computational complexity.

3.2. Complex-valued Shepp–Logan phantoms

To validate the proposed method on complex-valued data, we conducted experiments on two complex-valued numerical phantoms [17]. Each of them has a resolution of 128 × 128 pixels. The real parts and imaginary parts tend to be the similar but not exactly the same, which was used to validate the stability of the proposed method. The phantom images are piecewise smooth, where the TV or JTV would significantly increase the reconstruction accuracy. The sampling mask is single-slice [3,17] with variable density and reduction factor $R = 4$. Reconstructions were performed with BCS [17], GSMRI [14] and the proposed method.

3.3. Complex-valued turbo spin echo slices with early and late TEs

In vivo images were used to further validate the performance of the proposed method. These images were obtained with two different TE settings, using a TSE sequence (1 × 1 mm in-plane spatial resolution with 3 mm thick contiguous slices, TR = 6000 ms, TE1 = 27 ms, TE2 = 94 ms) [17]. This dataset contains 38 slices with 256 × 256 resolution. They are much less compressible than the previous two datasets. The sampling mask consisted of multiple radial lines [5,32–34] with reduction factor $R = 4$. Reconstructions were performed using BCS [17], GSMRI [14] and the proposed method.

4. Results

4.1. The benefit of group sparsity on both wavelet and gradient domains

Fig. 1 demonstrates the benefit of the proposed method when utilizing JTV and group wavelet sparsity on the SRI24 dataset. Comparing the proposed FJPG and conventional FPG [19], the JTV denoising is much more powerful on multi-contrast MR data. With more iterations, our algorithm achieves higher accuracy and less computational time. The results produced by the combination of group wavelet sparsity and JTV are always better than those produced by the group wavelet sparsity or JTV only. It confirms the benefit of the combination of group wavelet sparsity and JTV for multi-contrast CS-MRI.

4.2. SRI24 multi-channel brain atlas data

Fig. 2 depicts the SRI24 reconstruction results obtained by the conventional CS-MRI methods [3–6], multi-contrast MRI methods [17,14] and the proposed method. These images are very compressible. It is difficult to observe visible artifacts for all reconstruction

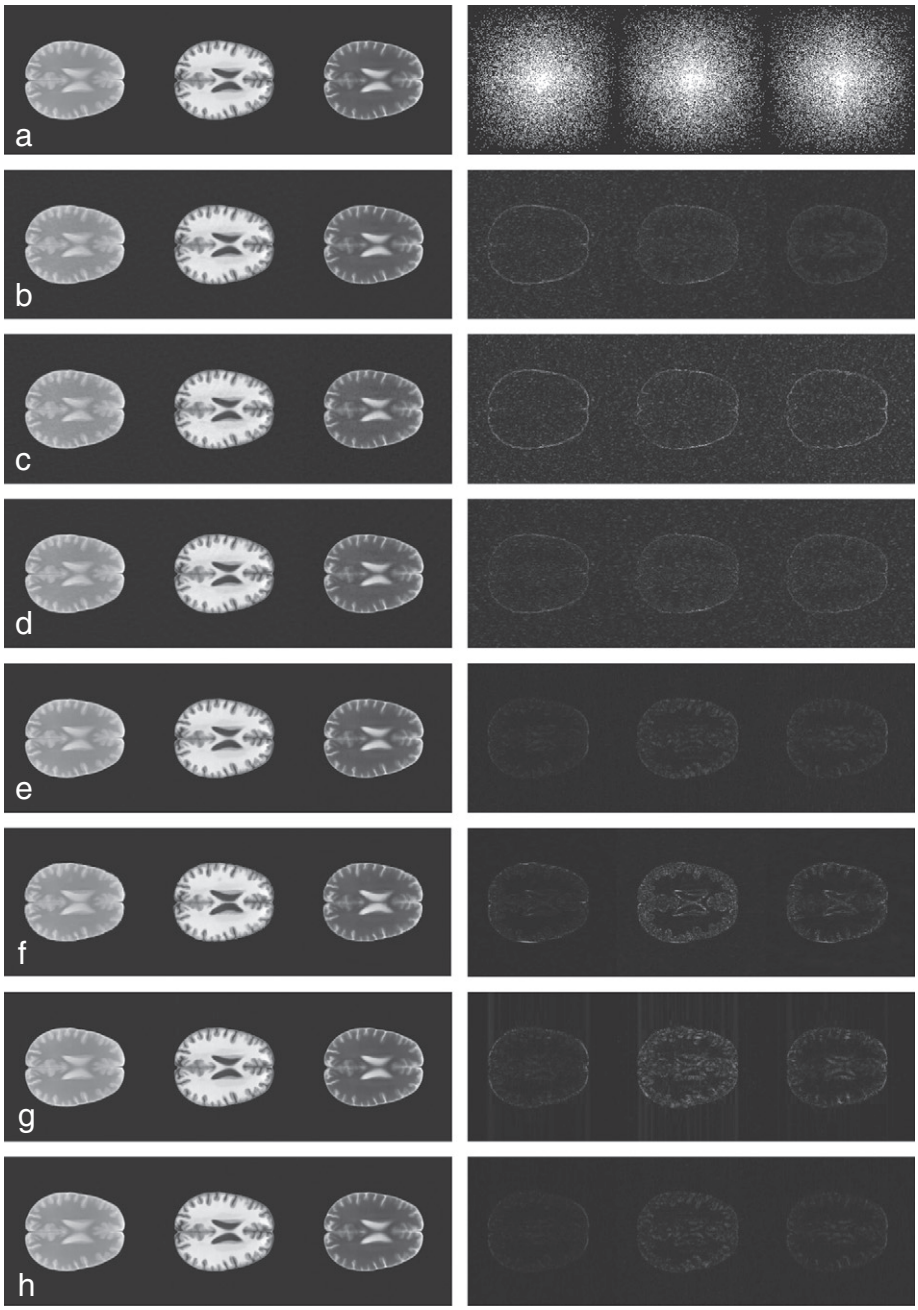

Fig. 2. Representative reconstruction results for SRI24 atlas images after undersampling with $R = 4$. a: Atlas images at Nyquist rate sampling (left) and the sampling masks (right). b–h: The reconstruction results (left) and the absolute errors (right) with SparseMRI [3], TVCMRI [4], RecPF [5], FCSA [6], BCS [17], GSMRI [14] and the proposed method, respectively.

results. For better visualization, the reconstruction errors are also shown on the same scale. We found the reconstruction with our method had the smallest error. Table 1 shows all the SNRs, REs as well as the reconstruction time for each algorithm. Our algorithm had the highest accuracy with comparable computational cost to the fastest CS-MRI algorithms. Due to the inherent shortcoming of the Bayesian CS framework [35], it has a huge computational cost that may make it practically impossible to use for most applications. GSMRI applies SPGL1 [36] to solve the group wavelet sparsity problem. It had similar accuracy with BCS on these data, while the computational cost was much less expensive.

Fig. 3 presents the convergence speed of each algorithm with convex relaxation in terms of iterations and CPU time. Inherent from the fast convergence rate of FISTA, FCSA and the proposed algorithm outperformed all other algorithms on this dataset. However, FCSA cannot reconstruct the multi-contrast MR images jointly, but only individually. That is why it is always inferior to the proposed method. In general, the conventional CS-MRI methods are not good as joint reconstruction methods, which has been also validated in previous works [17,14]. In later experiments, we only compared the proposed method with multi-contrast reconstruction methods [17,14].

Table 1
The SNRs, computational times and REs for the reconstructions in Fig. 2.

	SparseMRI	TVCMRI	RecPF	FCSA	BCS	GSMRI	Proposed
SNR (dB)	25.13	24.03	25.80	35.64	31.49	30.40	37.97
RE (%)	4.3	4.9	4.0	1.3	2.3	2.1	0.9
Time (s)	44.96	7.60	8.53	8.36	7134.1	11.81	8.78

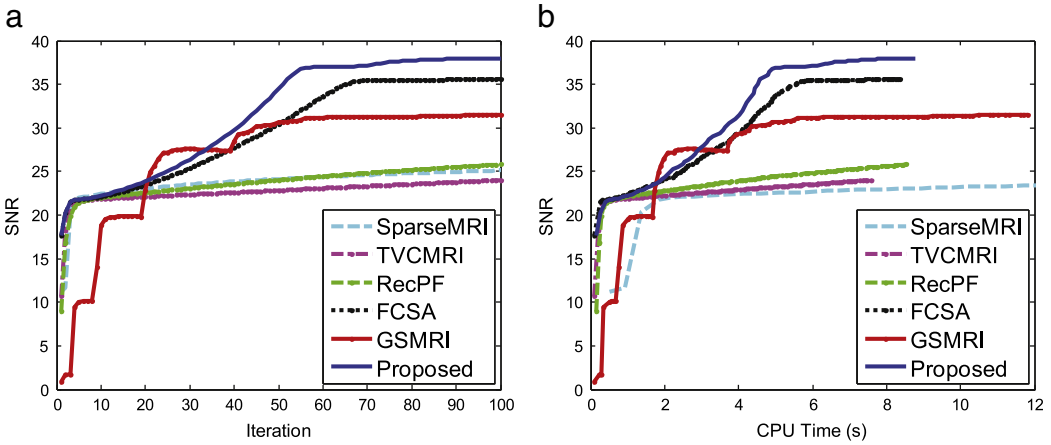

Fig. 3. Performance comparisons of reconstruction results for SRI24 atlas among algorithms with convex relaxation. a: SNR vs Iteration. b: SNR vs CPU time (s). Due to the high computational cost of SparseMRI, we only show its SNRs for the first 12 s.

4.3. Complex-valued Shepp–Logan phantoms

Absolute values of the reconstruction results after undersampling with $R = 4$ are presented in Fig. 4. The proposed method was better than BCS in terms of SNR and RE on this dataset, and far better than GSMRI. At the first glance, it seems that BCS achieved similar reconstruction results from visual observing. It is because such images are ideal examples for BCS, where the images are extremely piece-wise smooth. However, for in vivo data as we will show later, our method would be much more stable and robust. In addition, BCS

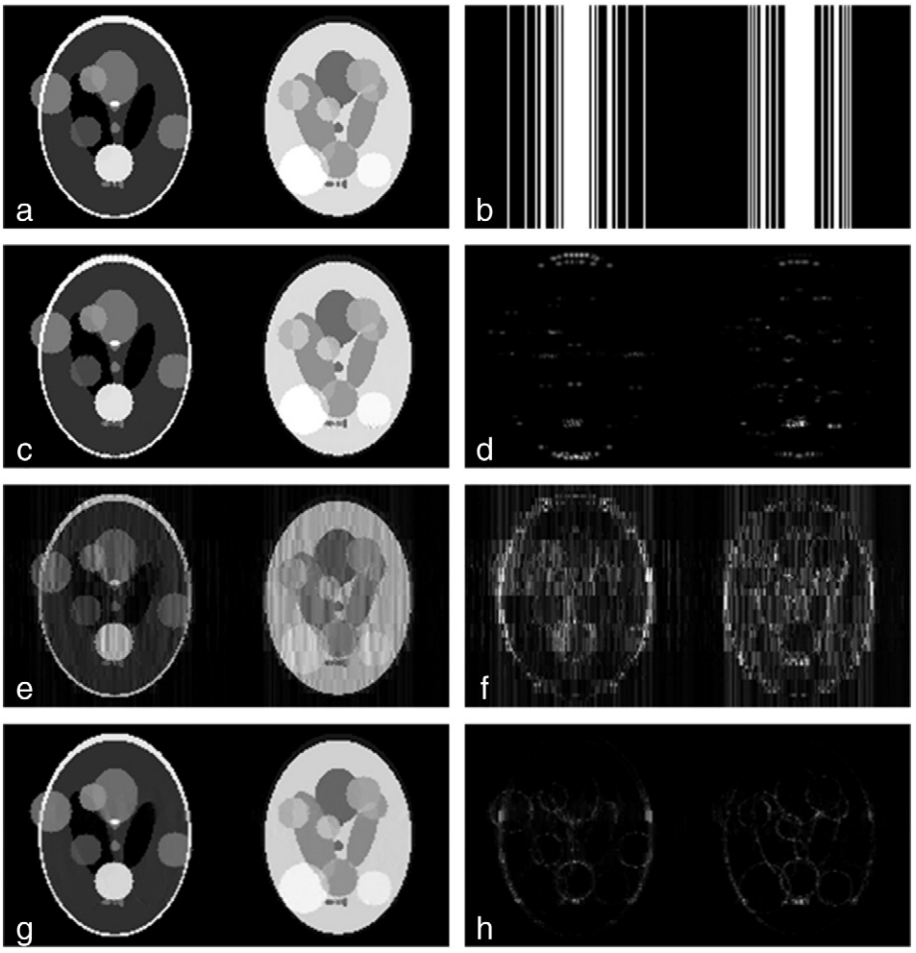

Fig. 4. Reconstruction results for the complex-valued Shepp–Logan phantoms after undersampling with reduction factor $R = 4$. a: Magnitudes of phantoms at Nyquist rate sampling. b: The sampling masks. c: The reconstruction result with Bayesian CS. Its SNR is 26.43. d: Absolute error of Bayesian CS reconstruction. RE = 4.3%. e: The reconstruction result with GSMRI. Its SNR is 14.32. f: Absolute error of GSMRI reconstruction. RE = 17.7%. g: The reconstruction result with the proposed method. Its SNR is 27.15. h: Absolute error of the proposed reconstruction. RE = 4.2%. The reconstruction times were: 271.2 s, 10.37 s, and 8.64 s, respectively.

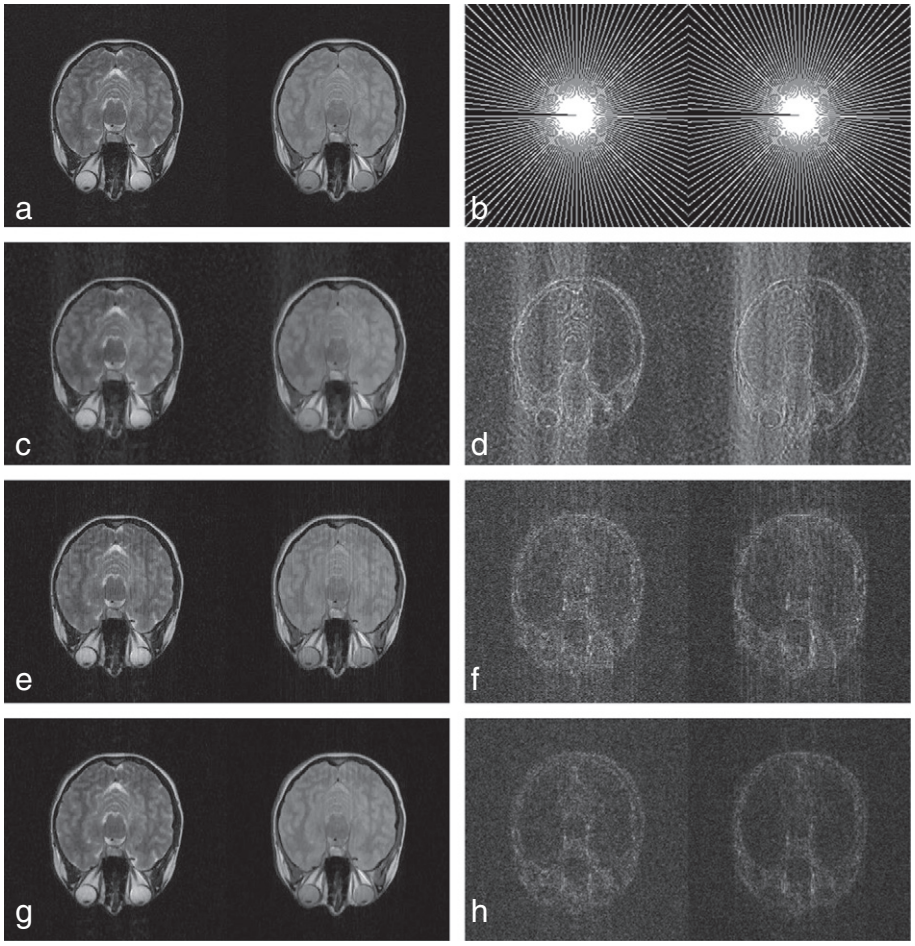

Fig. 5. Reconstruction results for the complex-valued in-vivo TSE images after undersampling with reduction factor $R = 4$. a: Magnitude images at Nyquist rate sampling. b: The sampling masks. c: The reconstruction result with Bayesian CS. Its SNR is 12.34. d: Absolute error of Bayesian CS reconstruction. RE = 27.4%. e: The reconstruction result with GSMRI. Its SNR is 15.07. f: Absolute error of GSMRI reconstruction. RE = 18.9%. g: The reconstruction result with the proposed method. Its SNR is 17.07. h: Absolute error of the proposed reconstruction. RE = 14.7%. The reconstruction times were: 10074.3 s, 18.21 s, and 12.04 s, respectively.

converges the fastest on these ideal images among all those used in experiments, but it is still substantially slower than our method. Visible artifacts can be found in the results reconstructed by GSMRI. This is because these images are piecewise smooth which is perfect for using gradient-based methods. However, it is still unknown how to combine TV or JTV in SPGL1 for GSMRI. Across different contrasts, the gradients and wavelet coefficients of these phantom images are not exactly the same, which validates the stability of the proposed method. When the sparsity patterns of different images tend to be the same, our algorithm can obtain very good results.

Table 2
Additional reconstruction results on the SRI24 and TSE datasets, with comparisons between GSMRI [14] and the proposed method.

Dataset	Schemes	R	GSMRI			Proposed		
			SNR (dB)	RE (%)	Time (s)	SNR (dB)	RE (%)	Time (s)
SRI24	Random (Fig. 2)	4	30.40	2.1	11.81	37.97	0.9	8.78
	Random	5	29.19	2.7	11.40	34.33	1.5	8.31
	Slice (Fig. 4)	3	22.16	6.1	11.65	26.54	3.7	8.68
	Slice	4	20.08	7.8	11.54	24.77	4.5	9.39
	Radial (Fig. 5)	4	28.98	2.8	11.58	33.63	1.6	9.06
	Radial	5	27.09	3.4	11.20	32.33	1.9	9.25
TSE	Random	3	17.86	14.0	18.88	19.08	12.0	12.85
	Random	4	16.26	16.4	17.86	17.08	13.7	11.47
	Slice	2	16.34	16.2	20.19	17.28	14.2	12.39
	Slice	3	13.33	22.3	18.30	14.38	19.4	11.51
	Radial	3	17.18	15.1	20.19	18.88	12.3	13.17
	Radial	4	15.07	18.9	18.21	17.07	14.7	12.04

4.4. Complex-valued turbo spin echo slices with early and late TEs

The reconstruction results on the in vivo human brain MRI data are shown in Fig. 5. These images are less compressible than the previous two datasets. With the same reduction factor, all algorithms performed worse on this dataset than they performed on the previous datasets. The result of BCS is significantly blurred on the edges, while the result of GSMRI contains obvious artifacts. By contrast, the result of our method is the closest to the original one. It takes more than 10,000 seconds for BCS for this reconstruction (it was still not converged yet), while our algorithm obtained an acceptable result within only around 12 seconds.

With the same datasets, additional reconstructions were performed to quantify the performance of the three multi-contrast MRI methods. The efficiency and effectiveness of the proposed method were validated under different sampling schemes with various reduction factors. The comparisons with GSMRI [14] are tabulated in Table 2, and the comparisons with BCS [17] are shown in Table 3. For speed, we used 128×128 low resolution images when comparing the results with BCS. For the same data, the results on the non-Cartesian masks were much better than those on the Cartesian mask.

Table 3
Additional reconstruction results on the SRI24 and TSE datasets, with comparisons between BCS [17] and the proposed method.

Dataset	Undersampling schemes	Reduction factor R	BCS			Proposed		
			SNR (dB)	RE (%)	Time (s)	SNR (dB)	RE (%)	Time (s)
SRI24	Random	3.5	32.29	2.0	2706.8	36.21	0.4	2.48
	Random	4	30.13	1.1	2129.9	33.53	0.6	2.46
	Slice	3	23.04	5.8	1919.8	24.68	4.8	2.02
	Slice	4	19.78	8.5	1838.4	20.70	7.6	2.09
	Radial	4	30.65	2.4	2384.4	32.72	1.9	2.15
	Radial	5	27.73	3.3	2335.0	29.82	2.6	2.09
TSE	Random	3	15.63	17.2	9262.7	23.87	6.7	3.25
	Random	4	12.95	23.1	5306.9	21.39	8.5	3.24
	Slice	3	15.44	16.0	177.6	15.72	15.1	2.65
	Slice	3.5	13.86	18.7	378.3	14.02	18.2	2.97
	Radial	3	15.91	16.5	3384.1	22.73	7.6	3.25
	Radial	4	13.52	21.3	4759.3	19.67	10.5	3.18

For speed, we used 128×128 low resolution images for these comparisons.

This is because the Cartesian sampling matrix is less incoherent. Also, with the same sampling scheme, the accuracy of each algorithm is higher with more measurements. When compared with different algorithms at the same condition (same sampling scheme and same reduction factor), our algorithm always outperformed the other two in terms of both reconstruction accuracy and computational complexity.

5. Discussion

One may note that there are two parameters that need to be tuned for most convex relaxation methods including the proposed method, while no parameter is required for BCS [17] and GSMRI [14]. Fortunately, the parameters are easy to tune when the sampling scheme is fixed. The parameters determine the relative weights between the least square fitting and the sparsity terms. The user could manually set how important the sparseness of the data is relative to the least squares fitting. However, BCS and GSMRI always seek the sparsest solution under a fixed tolerance of the least squares fitting, which may result in over-smoothing, especially for those less compressible images. The parameters to obtain the experiments results are set $\alpha = 0.01$ or 0.1, $\beta = 0.035$. Although they are not necessarily the optimal values, they were good enough to demonstrate the superiority of the proposed method. Interested readers may refer to existing methods [37,38] for more information on how to combine parallel imaging technique.

6. Conclusion

We have proposed an efficient algorithm for multi-contrast CS-MRI. The contributions of our work are as follows. First, we combined the group sparsity in both wavelet and gradient domains seamlessly and efficiently solved the combined problem, which is not available for existing multi-contrast CS-MRI methods. Second, the proposed algorithm has fast convergence speed borrowed from FISTA, and each iteration only costs $\mathcal{O}(TNlogN)$. These properties make real-time multi-contrast CS-MRI much more feasible than before. Finally, extensive experiments were conducted to show that the proposed method outperforms all conventional CS-MRI methods and two recent multi-contrast CS-MRI methods in terms of both accuracy and complexity.

Acknowledgments

The authors thank Dr. Berkin Bilgic for sharing the in vivo human brain data for the experiments in this article. The authors also thank all the authors for providing their codes online, which helped us a lot for the comparisons.

References

[1] Candès E, Romberg J, Tao T. Robust uncertainty principles: exact signal reconstruction from highly incomplete frequency information. IEEE Trans Inf Theory 2006;52(2):489–509.
[2] Donoho D. Compressed sensing. IEEE Trans Inf Theory 2006;52(4):1289–306.
[3] Lustig M, Donoho D, Pauly J. Sparse MRI: the application of compressed sensing for rapid MR imaging. Magn Reson Med 2007;58(6):1182–95.
[4] Ma S, Yin W, Zhang Y, Chakraborty A. An efficient algorithm for compressed MR imaging using total variation and wavelets. Proc. IEEE Conf. Computer Vision and Pattern Recognition (CVPR); 2008. p. 1–8.
[5] Yang J, Zhang Y, Yin W. A fast alternating direction method for TVL1-L2 signal reconstruction from partial Fourier data. IEEE J Sel Top Signal Process 2010;4(2):288–97.
[6] Huang J, Zhang S, Metaxas D. Efficient MR image reconstruction for compressed MR imaging. Med Image Anal 2011;15(5):670–9.
[7] Baraniuk R, Cevher V, Duarte M, Hegde C. Model-based compressive sensing. IEEE Trans Inf Theory 2010;56(4):1982–2001.
[8] Huang J, Zhang T, Metaxas D. Learning with structured sparsity. J Mach Learn Res 2011;12:3371–412.
[9] Huang J, Zhang T. The benefit of group sparsity. Ann Stat 2010;38(4):1978–2004.
[10] Cotter SF, Rao BD, Engan K, Kreutz-Delgado K. Sparse solutions to linear inverse problems with multiple measurement vectors. IEEE Trans Signal Process 2005;53(7):2477–88.
[11] Baron D, Duarte MF, Wakin MB, Sarvotham S, Baraniuk RG. Distributed compressive sensing, arXiv, preprint arXiv:0901.3403; 2009.
[12] Zelinski AC, Goyal VK, Adalsteinsson E. Simultaneously sparse solutions to linear inverse problems with multiple system matrices and a single observation vector. SIAM J Sci Comput 2010;31(6):4533–79.
[13] Yuan M, Lin Y. Model selection and estimation in regression with grouped variables. J R Stat Soc Ser B (Stat Methodol) 2006;68(1):49–67.
[14] Majumdar A, Ward R. Joint reconstruction of multiecho MR images using correlated sparsity. Magn Reson Imaging 2011;29:899–906.
[15] Majumdar A, Ward RK. Accelerating multi-echo t2 weighted MR imaging: analysis prior group-sparse optimization. J Magn Reson 2011;210(1):90–7.
[16] Majumdar A, Ward R. Rank awareness in group-sparse recovery of multi-echo MR images. Sensors 2013;13(3):3902–21.
[17] Bilgic B, Goyal V, Adalsteinsson E. Multi-contrast reconstruction with Bayesian compressed sensing. Magn Reson Med 2011;66:1601–15.
[18] Beck A, Teboulle M. A fast iterative shrinkage-thresholding algorithm for linear inverse problems. SIAM J Imaging Sci 2009;2(1):183–202.
[19] Beck A, Teboulle M. Fast gradient-based algorithms for constrained total variation image denoising and deblurring problems. IEEE Trans Image Process 2009;18(11):2419–34.
[20] Huang J, Chen C, Axel L. Fast multi-contrast MRI reconstruction. Proc. Medical Image Computing and Computer-Assisted Interventicon (MICCAI); 2012. p. 281–8.
[21] Chen C, Huang J. Compressive sensing MRI with wavelet tree sparsity. Proc. Adv. Neural Inf. Process. Syst. (NIPS); 2012. p. 1124–32.
[22] Chen C, Huang J. The benefit of tree sparsity in accelerated MRI. Med Image Anal 2014;18(6):834–42.
[23] Selesnick IW, Figueiredo MA. Signal restoration with overcomplete wavelet transforms: comparison of analysis and synthesis priors. Proc. SPIE 7446, Wavelets XIII; 2009. p. 74460D.
[24] Majumdar A, Ward RK. On the choice of compressed sensing priors and sparsifying transforms for MR image reconstruction: an experimental study. Signal Process Image Commun 2012;27(9):1035–48.
[25] Majumdar A, Ward RK. Synthesis and analysis prior algorithms for joint-sparse recovery. IEEE International Conference on Acoustics, Speech and Signal Processing (ICASSP); 2012. p. 3421–4.
[26] Bach F, Jenatton R, Mairal J, Obozinski G. Structured sparsity through convex optimization. Stat Sci 2012;27(4):450–68.
[27] Blomgren P, Chan TF. Color tv: total variation methods for restoration of vector-valued images. IEEE Trans Image Process 1998;7(3):304–9.
[28] Saito T, Takagaki Y, Komatsu T. Three kinds of color total-variation semi-norms and its application to color-image denoising. IEEE Int. Conf. Image Process. (ICIP); 2011. p. 1457–60.
[29] Chen C, Li Y, Huang J. Calibrationless parallel MRI with joint total variation regularization. Proc. Medical Image Computing and Computer-Assisted Intervention (MICCAI); 2013. p. 106–14.
[30] Rohlfing T, NM NZ, Sullivan E, Pfefferbaum A. The sri24 multichannel atlas of normal adult human brain structure. Hum Brain Mapp 2010;31:798–819.
[31] Cauley SF, Xi Y, Bilgic B, Setsompop K, Xia J, Adalsteinsson E, et al. Scalable and accurate variance estimation (save) for joint bayesian compressed sensing. 21th Annual Meeting of ISMRM; 2013. p. 2603.
[32] Chang T-C, He L, Fang T. MR image reconstruction from sparse radial samples using Bregman iteration. Proceedings of the 13th Annual Meeting of ISMRM, Seattle; 2006. p. 696.

[33] Ye J, Tak S, Han Y, Park H. Projection reconstruction MR imaging using FOCUSS. Magn Reson Med 2007;57(4):764–75.
[34] Block KT, Uecker M, Frahm J. Undersampled radial MRI with multiple coils. Iterative image reconstruction using a total variation constraint. Magn Reson Med 2007;57(6):1086–98.
[35] Ji S, Dunson D, Carin L. Multitask compressive sensing. IEEE Trans Signal Process 2009;57(1):92–106.
[36] Van Den Berg E, Friedlander M. Probing the Pareto frontier for basis pursuit solutions. SIAM J Sci Comput 2008;31(2):890–912.
[37] Liang D, Liu B, Wang J, Ying L. Accelerating SENSE using compressed sensing. Magn Reson Med 2009;62(6):1574–84.
[38] Weller D, Polimeni J, Grady L, Wald L, Adalsteinsson E, Goyal V. Combining nonconvex compressed sensing and grappa using the nullspace method. 18th Annual Meeting of ISMRM; 2010. p. 4880.